ADVANCED MATERIALS INTERFACES
Open Access
www.advmatinterfaces.de

Check for updates

# Critical Role of Surface Properties in Passive Interstitial Fluid Extraction Using Polymeric Hollow Microneedles for Wearable Diagnostics

*Ipek Atay, Emel Yilgör, Gürdeniz Neşer, Taher Abbasiasl, M. Baris Yagci, Iskender Yilgör, and Levent Beker**

**Efficient sampling of dermal interstitial fluid (ISF) is essential for continuous monitoring of biomarkers for early detection and management of chronic diseases. Transdermal ISF extraction using microneedles gained popularity due to their minimally invasive nature and efficient sampling capabilities. Among various ISF extraction modalities, passive extraction with hollow polymeric microneedles (HMN) stands out as an efficient, economical and user-friendly alternative that eliminates the need for external pumps or complex recovery processes. As passive HMN extraction relies on capillary action, influence of surface morphology and wettability of microchannels are investigated. In vitro ISF absorption capacities of HMNs fabricated by laser machining using polylactic acid (PLA), polymethyl methacrylate (PMMA) and polycarbonate (PC) are investigated. Microchannels are created on needle tips through micromachining with a 355 nm laser. Surface roughness induced by laser exposure is most prominent in PLA HMNs, which exhibited an absorption rate of 0.02 mg min$^{-1}$ per needle at an insertion force of 1.4 N per needle, while PMMA and PC-based HMNs showed rates of 0.01 mg min$^{-1}$ at 1.9 and 2.3 N per needle respectively. These findings highlight the critical influence of surface properties in enhancing the capillary action during passive ISF extraction with polymeric HMNs, supporting their potential integration into next-generation wearable biosensors.**

## 1. Introduction

Early identification of diseases and continuous health monitoring are crucial in improving human well-being and reducing healthcare expenses associated with treating preventable or manageable health conditions[1–8]. Diagnosing diseases and monitoring health requires the collection and examination of biomarkers and metabolites from bodily fluids. ISF is an ideal biofluid option for this purpose, compared to sweat or blood. ISF serves as a signaling, transport, and nourishment medium for the cells beneath the outermost layer of the epidermis[9–11]. Research indicates a significant similarity of proteins and other constituents between blood and ISF[9–16]. ISF sampling offers simpler and minimally invasive access to biomarkers compared to blood drawing techniques, eliminating the risk of coagulation and the need for specialist knowledge or skills[17,18].

Sampling ISF in large quantities remains challenging due to its low abundance per skin area, the risk of large molecule infiltration during the uptake (due to the viscoelastic properties of the dermal layers), negative pressure, and risks of biofouling in case of extended use.[17] ISF collection methods include reverse iontophoresis, micro dialysis suction blister, sonophoresis and microneedle extraction.[9] Most of these methods involve long sampling times, specialized equipment and require trained personnel.[9] Using needles longer than 16 mm can also be painful and uncomfortable.[9] Among these methods, ISF extraction by microneedles has become immensely popular. Microneedles (MNs) are a set of closely spaced needles that penetrate into the skin's outermost layer. They can be used to collect and monitor ISF from the skin in a minimally invasive way, with needle tips not exceeding 2–2.5 µm and not requiring specialized personnel.[9,19–21] ISF extraction with MNs offer a wide array of alternatives by using different materials and different nano/micro fabrication methods.

MN ISF collection modalities can be grouped as absorption via hydrogel MNs, active hollow microneedle (HMN) extraction and passive HMN extraction systems. Hydrogels are

I. Atay, E. Yilgör, G. Neşer, T. Abbasiasl, L. Beker
Department of Mechanical Engineering
Koç University
Istanbul 34450, Turkey
E-mail: lbeker@ku.edu.tr
I. Yilgör
Department of Chemistry
Koç University
Istanbul 34450, Turkey
E. Yilgör, M. B. Yagci, I. Yilgör
Surface Science and Technology Center (KUYTAM)
Koç University
Istanbul 34450, Turkey

The ORCID identification number(s) for the author(s) of this article can be found under https://doi.org/10.1002/admi.202500001

© 2025 The Author(s). Advanced Materials Interfaces published by Wiley-VCH GmbH. This is an open access article under the terms of the Creative Commons Attribution License, which permits use, distribution and reproduction in any medium, provided the original work is properly cited.

**DOI: 10.1002/admi.202500001**

hydrophilic crosslinked polymeric networks with high swelling capacity. Although ISF uptake with hydrogel MNs can be high since ISF can pass through the swollen network via passive diffusion, the recovery of the absorbed ISF for analysis is cumbersome, posing challenges for patient compliance.[21,22] The risk of degradation and subsequent loss of functionality as well as risk of biofouling are other disadvantages of hydrogel MN systems.[23,24] Active HMN extraction relies on mechanical components such as vacuum pumps to actively draw ISF through the hollow microneedle channel in large quantities. However, the complexity and the weight of the external pump systems bring a disadvantage.[25,26] The reliance on external power sources also imposes challenges such as extra weight and battery life.[27] Such components might result in discomfort during prolonged wear, which imposes a disadvantage for integration into wearable systems.[23] In contrast, passive hollow microneedles present a simple ISF absorption modality where ISF uptake is induced by capillary action, eliminating the need for external bulky or energy consuming components and reducing the overall size and complexity of the device.[23] In addition to simplified and cost-effective manufacturing process, this aesthetically pleasing design offers reduced footprint, ensuring patient comfort and compliance.[27,28] The integration of a colorimetric sensor assembled behind the needle array could also enable real-time monitoring of biomarkers without the need for cumbersome follow up procedures.[21,29] Passive HMNs were also shown to offer rapid and highly efficient biomarker sampling and analysis in various real-time biomarker monitoring studies.[27,29,30] The ability to integrate advanced sensing technologies, such as electrochemical sensors, enhances the diagnostic capabilities of these devices, paving the way for personalized healthcare solutions.[31]

A wide range of polymeric materials have been used for the fabrication of MNs, which include polyether ether ketone (PEEK),[19] PLA blends with polyvinyl alcohol (PVA),[32] PLA only,[33–35] polyvinyl pyrrolidone (PVP),[36] and polycarbonate (PC).[23] The choice of material plays critical roles on the simplicity and precision of the HMN design and fabrication, as well as its overall performance. Thus far HMNs have been developed utilizing materials such as glass,[12] silicon,[37,38] and metals,[39] which are biocompatible. However, their rigidity can lead to discomfort compared to more flexible and conformal alternatives. In the case of silicon and glass, their brittleness raises concerns about durability and mechanical failure during application. Synthetic polymers offer the advantage of tailorable surface and bulk properties, ensuring rapid and efficient ISF sampling while maintaining a flexible structure.[40] By utilizing advanced micro-stereolithography based 3D-printing fabrication techniques, it is possible to create polymeric HMNs with various geometries and tailorable surface and bulk properties. This allows the production of HMNs with greater affinity for or capacity to absorb ISF through capillary action.[41] Common methods for fabricating MNs from polymers include melt-processing, 3D printing, and laser-machining. These procedures can lead to differences in the mechanical characteristics, thermal behavior, and surface roughness of the polymers.[42,43] Polymer surfaces also exhibit an increase in surface roughness and polarity upon exposure to UV-laser irradiation.[43] It is well known that surface area generated by roughness has a positive effect on capillary action, which can lead to an increase in ISF uptake of HMNs.[41,44] Fabrication techniques such as 3D printing and compression molding may alter the morphology of thermoplastic polymers, leading to changes in their bulk and surface characteristics, which influence the absorption of ISF by HMNs.[19,20]

To mitigate the difficulty of ISF sampling via transdermal route due to the viscoelastic nature of the skin and negative pressure, different methods have been extensively studied to enhance surface properties and ISF absorption capacities of HMNs. Liu et. al., introduced surface PEGylation to obtain a hydrophilic coating on solid polymeric microneedles to improve their wettability and ISF absorption capacity.[45] Similarly, polydopamine coating was employed by Kim et. al., which resulted in an increase in the ISF absorption rate.[46] Al Sulaiman et. al., developed hydrogel coated microneedles for minimally invasive sampling of nucleic acids.[47]

The aim of this study was to investigate the influence of fabrication-induced surface changes generated during laser machining on the rate and amount of ISF absorption on HMNs fabricated using FDA approved biocompatible polymers, such as PMMA, PLA and PC, currently being used in many clinical applications.[48–53] Understanding the ISF-microneedle surface interactions is crucial for optimizing HMN designs for efficient ISF sampling. Although PLA based HMNs have been investigated for drug delivery, there are only a few studies for passive ISF uptake as it is considered a hydrophobic polymer with low affinity for ISF. PC is a biocompatible, hard, tough, transparent thermoplastic biomaterial, which is widely used in active ISF sampling due to ease of fabrication and high strength as part of pump-based extraction systems.[23,31] PMMA, an FDA-approved, hard, transparent thermoplastic biomaterial, has not been previously used for passive ISF sampling due to its hydrophobic behavior and brittle characteristics. Projection 3D micro-stereolithography was used to fabricate the master precision molds with photocurable resin material. The precision molds were utilized to produce MN molds using a crosslinked polydimethylsiloxane (silicone) resin, on which the polymeric MNs were fabricated by compression molding. The hollow channels on the needle tips were then produced by laser-machining. Surface wettability was measured before and after the fabrication steps. Theoretical ISF uptake was calculated using Young-Laplace equation, and the initial application force required to induce liquid uptake was determined using a compression force gauge and Z-stage set-up. In vitro absorption was measured using an agarose gel infused with synthetic ISF, and also Methylene blue (MB) dye solution, using a filter paper as a backing on the HMNs, where synthetic ISF was used to mimic the properties of the native ISF closely as possible and MB dye was utilized as a visual tracking component of liquid absorption of the HMNs. Spreading of the MB dye on the filter paper was measured and compared for each polymer. **Figure 1** summarizes the working principles, workflow and morphology of the HMN production and in vitro test process.

## 2. Results and Discussion

The development of polymeric HMN systems with improved passive ISF uptake through capillary action was investigated in this study. Figure 1 illustrates the overall concept, fabrication


© 2025 The Author(s). Advanced Materials Interfaces published by Wiley-VCH GmbH

21967350, 2025, 13, Downloaded from https://advanced.onlinelibrary.wiley.com/doi/10.1002/admi.202500001 by Koc University, Wiley Online Library on [10/11/2025]. See the Terms and Conditions (https://onlinelibrary.wiley.com/terms-and-conditions) on Wiley Online Library for rules of use; OA articles are governed by the applicable Creative Commons License

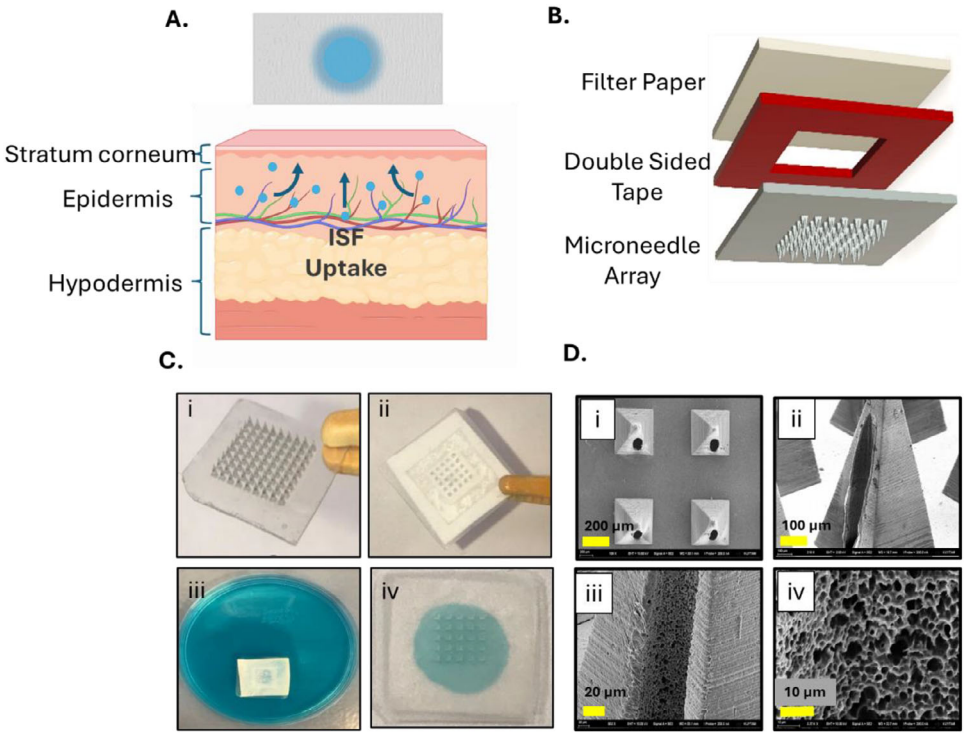



**Figure 1.** The schematics, workflow and morphology of the polymeric HMN ISF uptake systems. A) Schematics of colorimetric biomarker monitoring sensor application and the passive absorption HMN within the sensor system. B) The in vitro testing assembly of the HMNs with double sided tape and filter paper, C) Photographs of the HMNs (i, ii) before, and after filter paper assembly and (iii, iv) during and after in vitro absorption testing, and D) SEM images of the PLA HMNs at different magnifications (i) scale bar 200 µm, (ii) scale bar 100 µm, (iii) scale 20 µm and (iv) the morphology of the HMN channel walls (scale bar 10 µm).

workflow, and morphological characteristics of the HMN ISF uptake systems. The HMNs are integrated into a colorimetric biomarker monitoring sensor, where the passive absorption of ISF enables real-time analysis without the need for external power sources or complex equipment (Figure 1A). To simulate and evaluate the ISF uptake, we assembled an in vitro testing setup using double-sided tape and filter paper affixed to the back of the HMN arrays (Figure 1B,C). The HMNs exhibit precise geometrical features, as demonstrated by the scanning electron microscopy (SEM) images, which show the morphology of the hollow channels and the surface texture at various magnifications (Figure 1D). These structural characteristics are crucial, as they influence the capillary action responsible for passive ISF absorption.

### 2.1. Fabrication of the Polymeric Hollow Microneedles

In this study, we fabricated 7 × 7 and 5 × 5 arrays of microneedles with a needle length of 1.5 mm, a tip-to-tip distance of 1.2 mm, and a base distance of 0.6 mm, as shown in **Figure** 2A. The HMNs were produced by compression molding PLA, PMMA, and PC pellets onto silicone MN molds followed by laser-machining. Precision silicone MN molds were fabricated using projection 3D micro-stereolithography on MicroArch 320 BML printer (BMF Material Technology Inc., Shenzhen, China) with a photocurable resin. This technique allows the fabrication of intricate designs with high geometrical precision. Figure S1 (Supporting Information) gives images of the precision mold fabricated by the 3D projection micro-stereolithography, which was later used to produce the PDMS microneedle molds. To induce the capillary absorption for ISF uptake into the microneedles, microchannel bores with a diameter of ≈200 µm were drilled into the needle tips using an LPFK UV based laser with a wavelength of 355 nm, as shown in Figure 2B–F. The dimensional precision and reproducibility of laser drilling technique on microchannel fabrication can be observed via the microscopic images on Figure 2C,F.

Needle length is a crucial parameter in microneedle design. Needles that are too long can penetrate the skin at low angles, reaching deep into the capillary region, causing patient discomfort and risking contamination of ISF analytes with blood components. Conversely, needles that are too short may fail to reach below the stratum corneum layer.[23] A needle length of 1.5 mm was found to be optimal for accessing dermal ISF with minimal to no discomfort for patients.[9,23]

### 2.2. Surface Characterization of the Polymeric Hollow Microneedles

Surface roughness and surface energy play very important roles in ISF absorption. The interaction between the microneedle surface and the ISF directly influences the amount and rate of

 © 2025 The Author(s). Advanced Materials Interfaces published by Wiley-VCH GmbH

21967350, 2025, 13, Downloaded from https://advanced.onlinelibrary.wiley.com/doi/10.1002/admi.202500001 by Koc University, Wiley Online Library on [10/11/2025]. See the Terms and Conditions (https://onlinelibrary.wiley.com/terms-and-conditions) on Wiley Online Library for rules of use; OA articles are governed by the applicable Creative Commons License

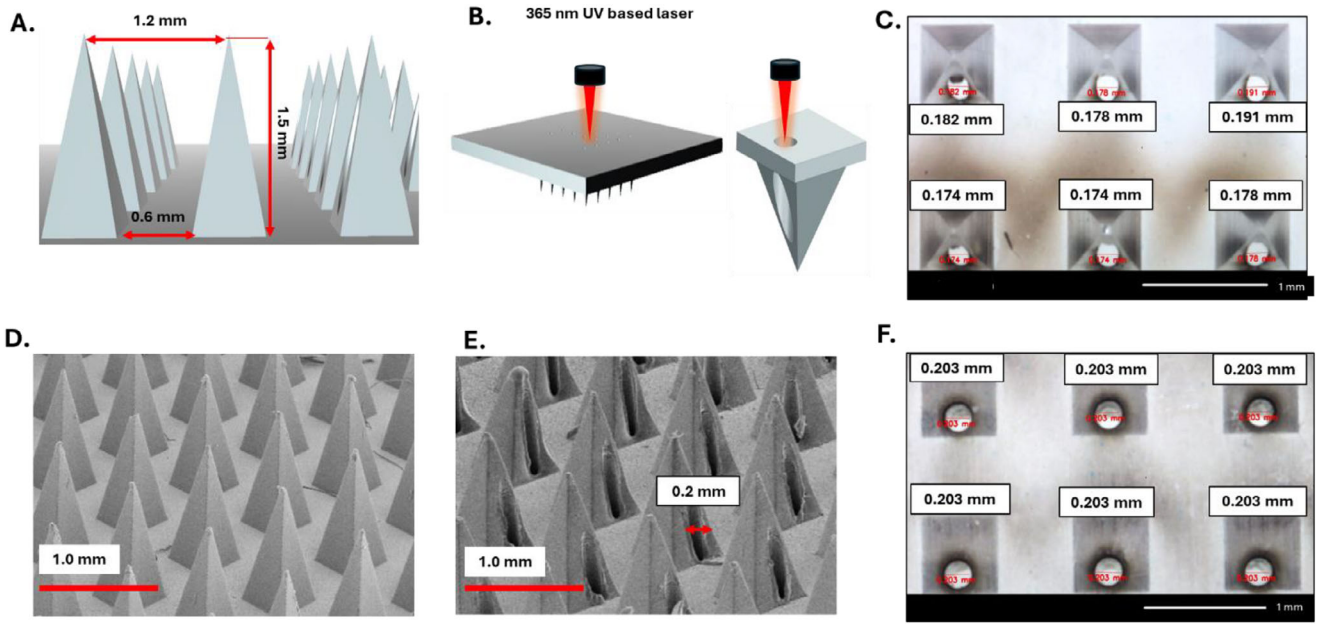



**Figure 2.** The fabrication steps of the HMNs. A) Schematic of the dimensions of the HMN design B) Laser machining process of the HMNs (C and F) C) Optical microscopy images of the top-view and (F) back-view of the microchannels (D and E) D) SEM image of the MN array before laser machining and E) SEM image of the laser machined HMNs (scale bars 1.0 mm).

absorption. Previous studies have shown that a static water contact angle of ≈60°, indicative of a moderately hydrophilic surface, is critical for effective ISF absorption.[54] The water affinity of polymer surfaces can be enhanced by various methods, including plasma or UV treatment, grafting with hydrophilic polymers such as surface PEGylation,[54] or increasing surface porosity with the addition of porogens.[32] Surface tension values of distilled water and ISF are 72 mN $m^{-1}$, whereas for methylene blue solution and PBS the values are 55 and 60 mN $m^{-1}$ respectively.[55] Polymers such as PLA, PMMA, and PC, with surface energies of 42, 41, and 46 mN $m^{-1}$ and water contact angles in 65–80° range[56–58] are expected to exhibit low surface wettability by water or aqueous systems, and consequently low ISF absorption capacity. **Figure 3** provides the detailed surface morphol-

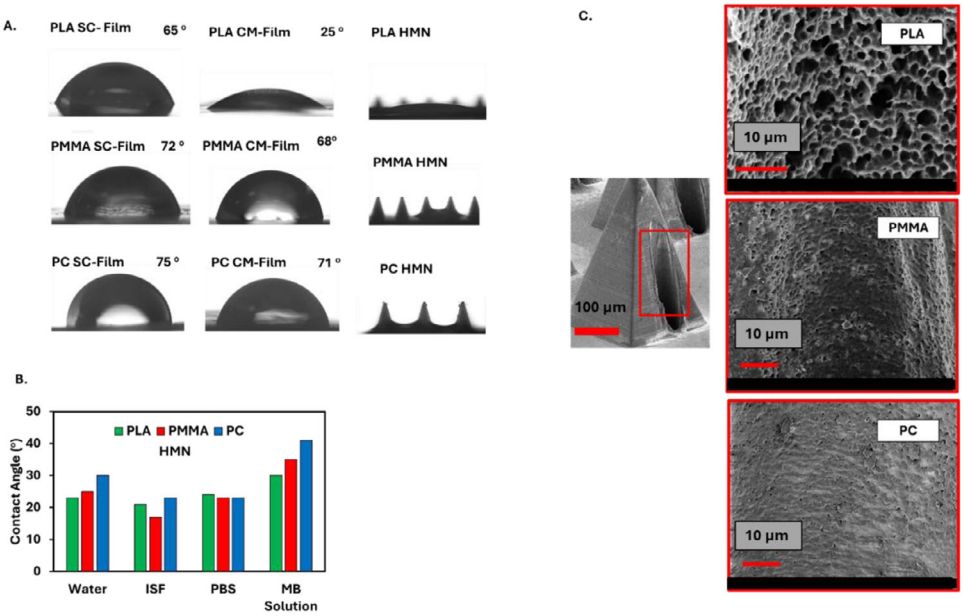



**Figure 3.** Surface morphology and surface wettability studies A) Images of the 5 µL water droplet spreading on solvent cast films (SC-Films), compression molded films (CM-Films) and HMNs. B) Contact angles measured on HMN surfaces with synthetic ISF, PBS, and MB dye solution C) SEM images of the porous structures within the PLA, PMMA, and PC HMN channel walls (scale bars are 10 µm).


© 2025 The Author(s). Advanced Materials Interfaces published by Wiley-VCH GmbH

21967350, 2025, 13, Downloaded from https://advanced.onlinelibrary.wiley.com/doi/10.1002/admi.202500001 by Koc University, Wiley Online Library on [10/11/2025]. See the Terms and Conditions (https://onlinelibrary.wiley.com/terms-and-conditions) on Wiley Online Library for rules of use; OA articles are governed by the applicable Creative Commons License

21967350, 2025, 13, Downloaded from https://advanced.onlinelibrary.wiley.com/doi/10.1002/admi.202500001 by Koc University, Wiley Online Library on [10/11/2025]. See the Terms and Conditions (https://onlinelibrary.wiley.com/terms-and-conditions) on Wiley Online Library for rules of use; OA articles are governed by the applicable Creative Commons License

ogy and wettability analysis results of the three different HMNs produced.

Fabrication of HMNs by laser-machining significantly influences surface properties compared to compression molded (CM) and solvent cast (SC) films. As shown in Figure 3A, solvent cast films of PLA, PMMA, and PC with very smooth surfaces displayed water contact angles of 65, 72, and 75°, respectively, indicating relatively hydrophobic surfaces. After laser machining, HMNs exhibited excellent wetting by distilled water, synthetic ISF, PBS, and 10 wt.% MB dye solution, with contact angles ≈ 20° (Figure 3B), clearly demonstrating the formation of highly hydrophilic surfaces. Increased hydrophilicity can be attributed to the chemical modifications on the PLA surface induced by laser irradiation. Laser exposure introduces polar functional groups such as hydroxyl (—OH), carbonyl (C═O), and carboxylic acid (—COOH) through surface oxidation and photodegradation of polymer backbone. These polar functional groups increase the surface free energy, creating hydrogen bonding with water molecules and hence reducing the water contact angle.[42,43,59] To investigate the changes in the surface chemical compositions of PLA, PC, and PMMA due to laser oxidation XPS studies were conducted. As can be seen in the XPS spectra provided in Figure S2 (Supporting Information), when compared with untreated surfaces, dramatic changes in the surface chemical compositions were observed in all polymers after laser treatment, where various new functional groups were observed. Increased hydrophilicity in all polymers investigated can be attributed to the formation of these surface functional groups.

Furthermore, laser-machining which produced well-defined hollow channels in microneedles (Figure 3C) also resulted in the formation of highly porous and rough surfaces within the HMN channel walls in all polymers, as also shown in Figure 3C. In addition to the chemical modification of surfaces ultraviolet laser radiation can also change the physical properties of the surfaces, such as its topography or geometrical structure and porosity, as reported by Rytlewski et.al.[43] Figures S3-S5 (Supporting Information) provide a detailed parametric study of the effect of laser power, mark speed, and repetition number on the average surface roughness of laser-treated and non-treated (neat) surfaces of each on PLA, PC, and PMMA CM films. The surface roughness values were obtained by laser scanning microscopy imaging on laser treated and untreated regions of the films. An increase in surface roughness in response to changing laser parameters was the most prominent in PLA sheets, where increasing laser power resulted in a dramatic increase in the roughness of the laser-treated regions, when compared with untreated regions. A decrease in mark speed, which is the time interval a region is exposed to the laser source in mm/s, also led to an increase on surface roughness of PLA sheets. As mark speed is decreased, the effect of laser treatment is expected to increase, as observed on PLA sheets. PMMA and PC exhibited similar behavior in their responses to changing laser parameters. Increasing repetition number, power and decreasing mark speed resulted in a smoothing effect on the laser treated regions versus untreated regions in PMMA and PC.

Increased surface roughness and total surface area of HMNs are expected to significantly enhance the capillary effect, thereby improving the performance of HMNs in terms of the rate and amount of ISF absorption.

### 2.3. Threshold Penetration Force Requirements for In Vitro Absorption and Mechanical Characterization of the Polymeric HMNs

To penetrate into the skin and induce the liquid absorption, a specific amount of force must be applied on the HMNs. Determining this threshold force on the in vitro skin-mimetic gel is essential for evaluating each HMN's mechanical robustness and suitability for in vitro applications. To assess the threshold force required to induce in vitro absorption and to determine the mechanical properties of HMNs, we designed a customized setup consisting of a Z-stage, a skin-mimetic agarose plate, and a force gauge, as shown in **Figure 4**. The threshold forces required for inducing liquid absorption by the PLA, PMMA, and PC HMNs were measured by inserting the 7 × 7 needle arrays into the skin-mimetic agarose gel infused with 10 wt.% methylene blue dye. The agarose plate was placed on the Z-stage of the mechanical test setup (Figure 4A), and the HMNs were attached to the force probe using a plexiglass holder, with the tips facing downward. The stage was moved upward until the first liquid uptake and spread was observed on the filter paper. The corresponding force readings for the first liquid absorption were 1.40 N for PLA, 1.93 N for PMMA and 2.30 N for PC, as shown in Figure 4B. To obtain a more comprehensive overview on the utilization range of the HMNs, cyclic insertion-removal experiments were performed using the same Z-stage set up on skin mimetic parafilm covered agarose gel system. Parafilm is a commonly used material to represent the viscoelastic properties of the stratum corneum upper part of the skin.[23] As shown in Force versus Number of Insertion (or cycle number) plots provided in Figure S6 (Supporting Information), the force required to penetrate into the skin mimetic system increased only slightly even after 10 insertion-removal cycles.

To assess the mechanical properties of the HMNs, a constant compression force of 10 N was applied at a speed of 5 μm $s^{-1}$ speed on the 7 × 7 HMN arrays. Previous studies have found that the minimum force required to penetrate the skin for ISF collection is approximately 0.08 N per needle.[54] All three types of polymeric HMNs investigated in this study exhibited mechanical robustness at 0.2 N per needle, far exceeding the minimum requirement. The smooth force-displacement curves shown in Figure 4C indicate that the HMNs maintain mechanical stability under 10 N compression without breaking.

Since the intrinsic capillary absorption properties depend on surface energy, the theoretical capillary absorption pressure differs for each polymer. To calculate the theoretical ISF uptake, we applied the Young-Laplace equation, according to the study conducted by Turner et. al.:[15]

$$\Delta P = (2\gamma \cos\theta)\,/a \tag{1}$$

where $\Delta P$ is the capillary pressure difference, $a$ is the radius of the capillary, $\gamma$ is the surface tension of the liquid, and $\theta$ is the static water contact angle of the polymer surface. From the $\Delta P$, the height $h$ of ISF moving upward inside the microneedle channel can be calculated using:

$$h = \Delta P/\rho g \tag{2}$$

 © 2025 The Author(s). Advanced Materials Interfaces published by Wiley-VCH GmbH

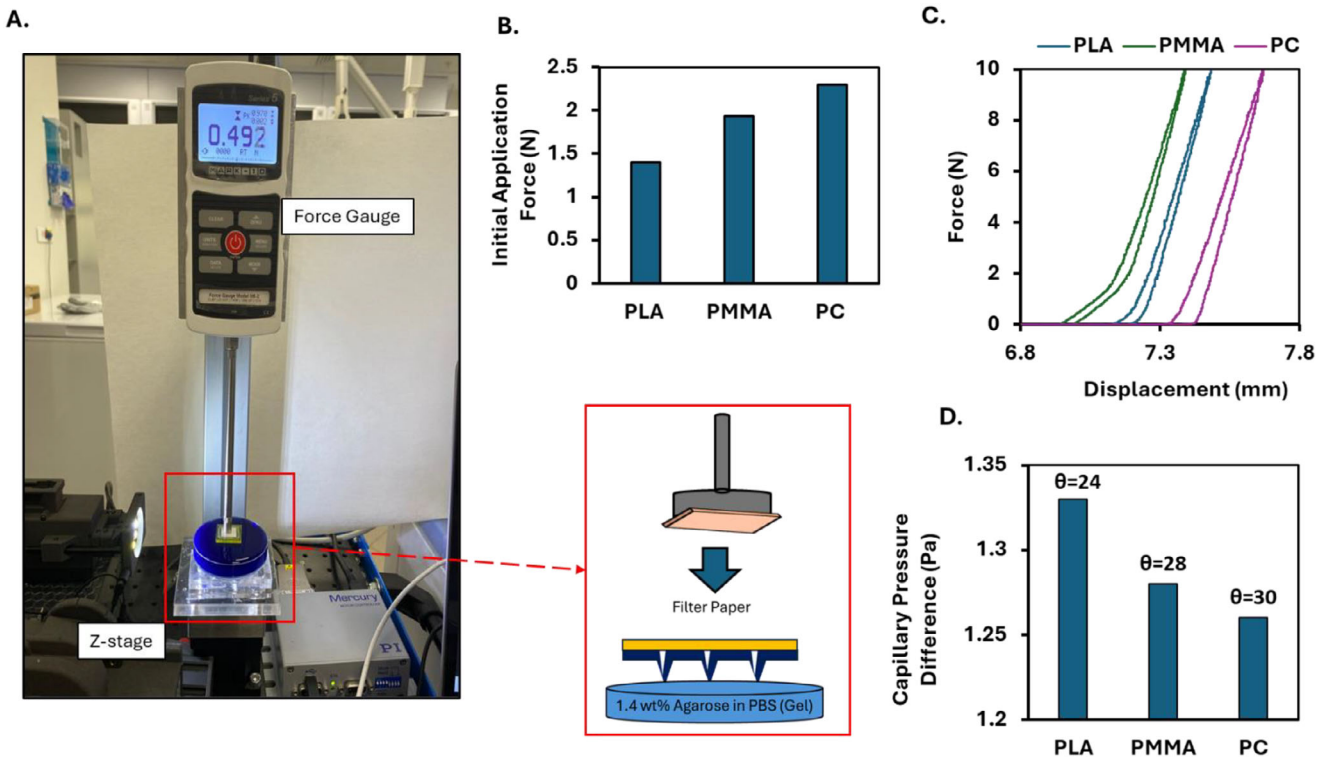



**Figure 4.** Mechanical characterization and the theoretical capillary pressure difference of the HMNs A) Photographic image of the mechanical test set-up B) The application force required to induce liquid absorption for the three polymers C) The force-displacement curves of the three polymers under 10 N compression force and D) Theoretical capillary pressure differences of the three polymers and static water contact angles measured.

where $\rho$ is the density of ISF (≈0.997 g $cm^{-3}$) and $g$ is the gravitational acceleration (9.8 m $s^{-2}$). The PLA HMN was found to exhibit the highest capillary pressure difference of 1.33 Pa followed by 1.28 Pa for PMMA and 1.26 Pa for PC (Figure 4D). These theoretical results align with the threshold force requirements discussed above.

The in vitro liquid absorption rate and time-based spread of the MB dye solution on the filter paper backing layer are important parameters for assessing the passive absorption performance of each polymer. MB dye was utilized as a visual tracking element for fluid movement within the microneedle channels and confirmation of dye absorption. MB has been widely used as a simple quantification molecule for initial proof of concept experiments in previous studies.[23] Synthetic ISF was prepared as a representative of the native ISF, as described previously in literature.[60] Time dependent in vitro absorption rates of MB dye and synthetic ISF by all three HMN systems were presented in **Figure 5**. Photographs capturing the time-based spreading of MB dye were taken at the indicated time intervals (Figure 5B). The absorption rate of each polymeric HMN was determined by weighing the 5 × 5 HNM arrays before and after insertion into the skin-mimetic agarose plate for 30 min at 37 °C (Figure 5A,C).

PLA based HMNs exhibited the largest spread diameter of the aqueous MB dye at each time interval, followed by PMMA and PC. PLA HMNs also demonstrated the highest absorption rate among the three polymers. These results correspond well with the surface polarities of the HMN assemblies based on the static water contact angle values provided in Figure 3A.

## 3. Conclusion

HMNs are efficient, low-cost, and user-friendly alternatives for passive ISF extraction. In this study, we successfully fabricated and characterized HMNs using three different hydrophobic polymeric resins, PLA, PMMA, and PC, each with different polarities and capacities for passive ISF absorption. We compared the ISF absorption capacities of these polymeric HMNs in terms of their polarities and the surface morphologies after introducing laser-machined microchannels. Laser machining was found to induce different surface roughness features and wettability profiles on HMNs, influencing their absorption performance. HMNs with the highest porosities were obtained from PLA, followed by PMMA and PC. The results indicate that PLA HMNs exhibit superior surface wettability and ISF absorption rates compared to PMMA and PC, suggesting their potential application for effective biomarker monitoring. These findings pave the way for further exploration of these polymers as viable materials for HMNs, potentially expanding the range of applications in minimally invasive diagnostics. Various research groups have successfully implemented microneedles within electrochemical or colorimetric biosensing platforms. In these systems, passive or actively extracted ISF is analyzed via electrochemical biosensors such as enzymatic sensors for glucose or lactate or colorimetric sensors.[9,23,61] Conductive inks and adhesive patches made from polymers such as thermoplastic polyurethanes are used to achieve electrical conductivity, signal transmission and skin conformity.[21,23,61] Challenges in achieving the development of


© 2025 The Author(s). Advanced Materials Interfaces published by Wiley-VCH GmbH

21967350, 2025, 13, Downloaded from https://advanced.onlinelibrary.wiley.com/doi/10.1002/admi.202500001 by Koc University, Wiley Online Library on [10/11/2025]. See the Terms and Conditions (https://onlinelibrary.wiley.com/terms-and-conditions) on Wiley Online Library for rules of use; OA articles are governed by the applicable Creative Commons License

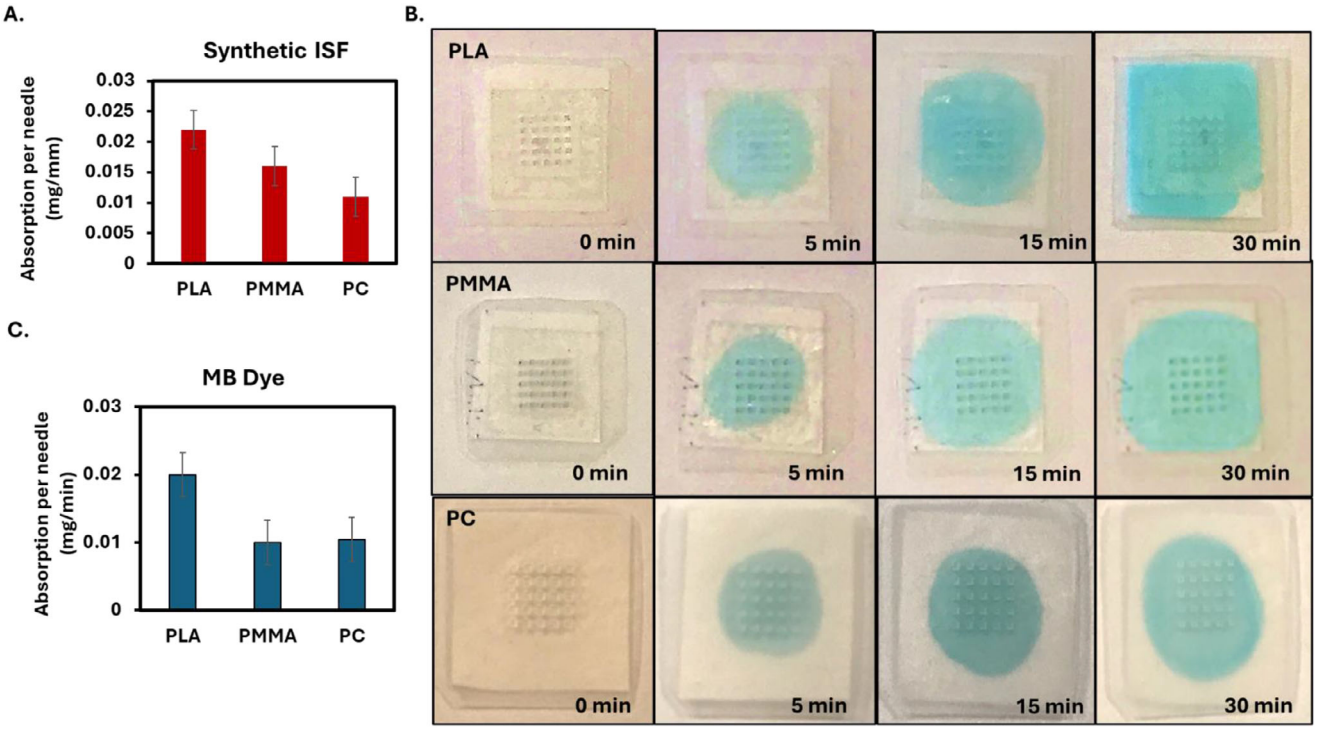



**Figure 5.** The time-based absorption measurements of synthetic ISF and MB dye and photographic images of the spreading of MB dye solution on the filter paper backing of the three polymeric HMN assemblies A) Synthetic ISF absorption rates of each polymeric HMN per needle plotted against time B) Photographic images of the spreading of the aqueous methylene blue dye over 30 mins for each polymeric HMN, and C) MB dye absorption rates of each polymeric HMN per needle.

microneedle-based sensing platforms include ISF extraction stability over extended durations, biofouling risks, long term skin compatibility, possible motion artifact elimination, as well as issues with wireless data transmission.[9,21,23,61] As with any novel biomedical instrumentation development, integration of different disciplines such as mechanical, electrical and materials science and engineering is imperative to overcome such challenges when translating microneedle-based sensing systems from lab bench to real life clinical applications.

Our results demonstrate that passive ISF extraction with HMNs using FDA-approved hydrophobic polymers after laser surface treatment is feasible for colorimetric sensing and other ISF sampling applications where minimal ISF uptake is sufficient. This approach eliminates the need for complex active-pump or hydrogel absorption methods with cumbersome recovery procedures. As the next-generation wearable diagnostic devices progress toward mobile and visual-based real time biomarker analysis, passive polymeric HMN systems will become invaluable components due to their efficiency and sustainability.

## 4. Experimental Section

*Materials*: PLA, PMMA and PC resins were obtained from Natureworks, Goodfellow, and Sabic respectively. All polymers were used as received. BIO resin was a product of BMF. Deionized and double distilled water was produced in our laboratory. RTV silicone resin (Sylgard 184 Silicone Elastomer) was obtained from Dow Corning MI, USA. Agarose from Merck was used as received. Dichloromethane and toluene were obtained from Merck and used as received. Methylene Blue (MB) dye was obtained from Sigma Aldrich. Synthetic ISF was prepared in our laboratories according to previous studies.[62–71]

*Methods—Design and 3D Printing of Microneedle Molds*: Microneedle geometries with pyramid needle shapes and tip-to-tip distance of 12 mm and a height of 1.5 mm were designed using CAD software with 0.6 mm spacing. The thickness of the MN patch was 2 mm. To prepare the female silicone mold, a master male mold was fabricated with a MicroArch S230 3D printer (BMF Material Technology Inc., Shenzhen, China) using Bioresin. PDMS resin and its curing agent were mixed at 10:1 ratio, stirred well and subsequently vacuumed at 23 °C for 30 min. PDMS resin mixture was cast onto the 3D printed male master mold and cured at 100 °C for 2 h, to produce silicone mold with inverted MN tips.

*Fabrication of Microneedles*: PLA, PMMA, and PC pellets were placed onto the silicone mold and heated up to 200, 230, and 300 °C respectively for 30 min. Then a 1 kg weight was applied to pressurize and spread the molten polymer granules evenly inside the mold and fill the needle tips. After 30 min, the weight was removed, and the mold was cooled down to room temperature to ensure complete solidification of the MN patches (CM films). To obtain solvent cast (SC) films, PLA and PC pellets were dissolved in dichloromethane and PMMA pellets in toluene at ambient temperature to obtain 20 wt.% polymer solutions. The solutions were solvent-cast on Teflon molds to obtain films with smooth surfaces for comparative surface wettability measurements.

*Fabrication of Hollow Geometries by Laser Machining*: To induce ISF uptake by capillary action, microchannels with a diameter of 200 µm were drilled within each needle tip of the MN patches by a UV-based laser-cutting device (Protolaser U4; LPKF, Germany). The parameters for successful drilling for PLA HMNs were 7.3 kW, 24 µJ pulse energy 150 mm $s^{-1}$ speed for 300 Hz frequency and 400 repetition, where for PMMA and PC

 © 2025 The Author(s). Advanced Materials Interfaces published by Wiley-VCH GmbH

21967350, 2025, 13, Downloaded from https://advanced.onlinelibrary.wiley.com/doi/10.1002/admi.202500001 by Koc University, Wiley Online Library on [10/11/2025]. See the Terms and Conditions (https://onlinelibrary.wiley.com/terms-and-conditions) on Wiley Online Library for rules of use; OA articles are governed by the applicable Creative Commons License

the parameters used were 150 Hz frequency, 3.6 kW power, 24 µJ energy at 300 mm $s^{-1}$ speed and 150 repetition.

*Surface Characterization Methods*: The surface wettability of the HMNs, CM films and SC films were measured on a Krüss G-10 goniometer with 5 µL droplet of distilled water at ambient temperature, 23 ± 2 °C. For SEM measurements, the HMNs were coated with 50 nm gold to ensure conductivity and were then imaged at 10 kV, with working distance 33.8 mm on Zeiss Ultra Plus Field Emission Scanning Electron Microscope. Surface roughness of laser treated and untreated CM films were measured on OLYMPUS LEXT™ OLS5100 3D laser scanning microscope. Surface chemistry of the laser treated and untreated CM films were measured on Thermo K-Alpha X-Ray photoelectron spectrometer.

*Mechanical Characterization of the Microneedle Patches*: The mechanical properties of the MN patches were investigated using a custom force-displacement set-up consisting of MARK-10 Force Gauge and Z- axis stage. The patches were placed on the *Z*-axis stage with needles facing upward, while the vertical force of 10 N was applied on the tip of needles with step size of 5 µm and at a rate of 0.05 µm $s^{-1}$. To measure the threshold force required to induce absorption in the HMNs, the 7 × 7 needle-array HMN patches were placed under the force gauge and placed above the skin-mimetic 10 wt.% MB dye-infused agarose gel on the Z-stage and gradually inserted inside the gel. The force readings observed upon the first visual confirmation of the dye spread on the filter paper was recorded as the initial application force.

*In Vitro ISF Absorption (detection) from Agarose Hydrogel*: Agarose gel (1.4 wt.% agarose + 98.6wt.% phosphate buffer solution to mimic ISF) covered with a water-impermeable parafilm (mimicking the stratum corneum) was used as the artificial skin model to investigate the ability of HMNs to extract ISF. The HMN patches were inserted into the skin-mimetic agarose gel on the Z-stage and visual photographs and weight measurements were recorded at every 5, 10 and 30 min.

## Supporting Information

Supporting Information is available from the Wiley Online Library or from the author.

## Acknowledgements

This research was funded by the European Research Council (2ND-CHANCE, grant no. 101043119). The authors acknowledge Koç University Surface Science and Technology Center (KUYTAM) and Koç University Nanofabrication and Nanocharacterization Center (N2Star).

## Conflict of Interest

There is an ongoing patent application.

## Data Availability Statement

The data that support the findings of this study are available in the supplementary material of this article.

## Keywords

hollow microneedles, Passive ISF sampling, wearable biosensors

Received: January 3, 2025
Revised: May 14, 2025
Published online: June 3, 2025

[1] F. Haghayegh, A. Norouziazad, E. Haghani, A. A. Feygin, R. H. Rahimi, H. A. Ghavamabadi, D. Sadighbayan, F. Madhoun, M. Papagelis, T. Felfeli, R. Salahandish, *Adv. Sci.* **2024**, *11*, 2400595.
[2] A. A. Smith, R. Li, Z. T. Tse, *Sci. Rep.* **2023**, *13*, 4998.
[3] H. C. Ates, P. Q. Nguyen, L. Gonzalez-Macia, E. Morales-Narváez, F. Güder, J. J. Collins, C. Dincer, *Nat. Rev. Mater.* **2022**, *7*, 887.
[4] H. Wang, Y. Zhang, X. Liang, Y. Zhang, *ACS Nano* **2021**, *15*, 12497.
[5] Y. Lin, M. Bariya, A. Javey, *Adv. Funct. Mater.* **2021**, *31*, 2008087.
[6] M. Parrilla, K. De Wael, *Adv. Funct. Mater.* **2021**, *31*, 2107042.
[7] H. Teymourian, M. Parrilla, J. R. Sempionatto, N. F. Montiel, A. Barfidokht, R. Van Echelpoel, K. De Wael, J. Wang, *ACS Sens.* **2020**, *5*, 2679.
[8] T. M. Dall, W. Yang, K. Gillespie, M. Mocarski, E. Byrne, I. Cintina, K. Beronja, A. P. Semilla, W. Iacobucci, P. F. Hogan, *Diabetes Care* **2019**, *42*, 1661.
[9] K. M. Saifullah, Z. Faraji Rad, *Adv. Mater. Interfaces* **2023**, *10*, 2201763.
[10] H. Teymourian, A. Barfidokht, J. Wang, *Chem. Soc. Rev.* **2020**, *49*, 7671.
[11] J. Heikenfeld, A. Jajack, B. Feldman, S. W. Granger, S. Gaitonde, G. Begtrup, B. A. Katchman, *Nat. Biotechnol.* **2019**, *37*, 407.
[12] P. M. Wang, M. Cornwell, M. R. Prausnitz, *Diabetes Technol. Therapeut.* **2005**, *7*, 131.
[13] F. Tehrani, H. Teymourian, B. Wuerstle, J. Kavner, R. Patel, A. Furmidge, R. Aghavali, H. Hosseini-Toudeshki, C. Brown, F. Zhang, K. Mahato, *Nat. Biomed. Eng.* **2022**, *6*, 1214.
[14] P. P. Samant, M. M. Niedzwiecki, N. Raviele, V. Tran, J. Mena-Lapaix, D. I. Walker, E. I. Felner, D. P. Jones, G. W. Miller, M. R. Prausnitz, *Sci. Transl. Med.* **2020**, *12*, aaw0285.
[15] Y. Cheng, X. Gong, J. Yang, G. Zheng, Y. Zheng, Y. Li, Y. Xu, G. Nie, X. Xie, M. Chen, C. Yi, *Biosens. Bioelectron.* **2022**, *203*, 114026.
[16] X. Li, X. Huang, J. Mo, H. Wang, Q. Huang, C. Yang, T. Zhang, H. J. Chen, T. Hang, F. Liu, L. Jiang, *Adv. Sci.* **2021**, *8*, 2100827.
[17] M. Friedel, I. A. Thompson, G. Kasting, R. Polsky, D. Cunningham, H. T. Soh, J. Heikenfeld, *Nat. Biomed. Eng.* **2023**, *7*, 1541.
[18] H. Chang, M. Zheng, X. Yu, A. Than, R. Z. Seeni, R. Kang, J. Tian, D. P. Khanh, L. Liu, P. Chen, C. Xu, *Adv. Mater.* **2017**, *29*, 1702243.
[19] M. Parrilla, U. Detamornrat, J. Domínguez-Robles, R. F. Donnelly, K. De Wael, *Talanta* **2022**, *249*, 123695.
[20] L. Zhao, C. Zhang, J. M. Abu-Ershaid, M. Li, Y. Li, Y. Naser, X. Dai, M. T. Abbate, R. F. Donnelly, *Adv. Healthcare Mater.* **2021**, *10*, 2100996.
[21] H. Teymourian, F. Tehrani, K. Mahato, J. Wang, *Adv. Healthcare Mater.* **2021**, *10*, 2002255.
[22] R. He, Y. Niu, Z. Li, A. Li, H. Yang, F. Xu, F. Li, *Adv. Healthcare Mater.* **2020**, *9*, 1901201.
[23] T. Abbasiasl, F. Mirlou, H. Mirzajani, M. J. Bathaei, E. Istif, N. Shomalizadeh, R. E. Cebecioğlu, E. E. Özkahraman, U. C. Yener, L. A Beker, *Adv. Mater.* **2024**, *36*, 2304704.
[24] S. Zhou, Y. Chino, T. Kasama, R. Miyake, S. Mitsuzawa, Y. Luan, N. B. Ahmad, H. Hibino, M. Takai, *ACS Nano* **2024**, *18*, 26541.
[25] M. A. Lopez-Ramirez, F. Soto, C. Wang, R. Rueda, S. Shukla, C. Silva-Lopez, D. Kupor, D. A. McBride, J. K. Pokorski, A. Nourhani, N. F. Steinmetz, *Adv. Mater.* **2020**, *32*, 1905740.
[26] P. R. Miller, X. Xiao, I. Brener, D. B. Burckel, R. Narayan, R. Polsky, *Adv. Healthcare Mater.* **2014**, *3*, 876.
[27] J. Bai, D. Liu, X. Tian, Y. Wang, B. Cui, Y. Yang, S. Dai, W. Lin, J. Zhu, J. Wang, A. Xu, *Sci. Adv.* **2024**, *10*, adl1856.
[28] B. Ciui, A. Martin, R. K. Mishra, B. Brunetti, T. Nakagawa, T. J. Dawkins, M. Lyu, C. Cristea, R. Sandulescu, J. Wang, *Adv. Healthcare Mater.* **2018**, *7*, 1701264.
[29] Z. Li, Y. Wang, R. Zhang, Z. Liu, Z. Chang, Y. Deng, X. Qi, *ACS nano* **2024**, *18*, 23876.
[30] J. Lölsberg, A. Cinar, D. Felder, G. Linz, S. Djeljadini, M. Wessling, *Small* **2019**, *15*, 1901356.
[31] X. Luo, L. Yang, Y. Cui, *Biomed. Microdevices* **2023**, *25*, 20.


© 2025 The Author(s). Advanced Materials Interfaces published by Wiley-VCH GmbH

21967350, 2025, 13, Downloaded from https://advanced.onlinelibrary.wiley.com/doi/10.1002/admi.202500001 by Koc University, Wiley Online Library on [10/11/2025]. See the Terms and Conditions (https://onlinelibrary.wiley.com/terms-and-conditions) on Wiley Online Library for rules of use; OA articles are governed by the applicable Creative Commons License

[32] L. Bao, J. Park, B. Qin, B. Kim, *Sci. Rep.* **2022**, *12*, 10693.
[33] Q. L. Wang, D. D. Zhu, Y. Chen, X. D. Guo, *Mater. Sci. Eng. C* **2016**, *65*, 135.
[34] A. Khosraviboroujeni, S. Z. Mirdamadian, M. Minaiyan, A. Taheri, *Drug Deliv. Transl. Res.* **2022**, *12*, 1195.
[35] S. Terashima, C. Tatsukawa, M. Suzuki, T. Takahashi, S. Aoyagi, *Precision Eng.* **2019**, *59*, 110.
[36] J. S. Kim, J. A. Choi, J. C. Kim, H. Park, E. Yang, J. S. Park, M. Song, J. H. Park, *Int. J. Pharm.* **2020**, *591*, 119928.
[37] E. V. Mukerjee, S. D. Collins, R. R. Isseroff, R. L. Smith, *Sensors Actuators A, Phys.* **2004**, *114*, 267.
[38] Y. Li, H. Zhang, R. Yang, Y. Laffitte, U. Schmill, W. Hu, M. Kaddoura, E. J. Blondeel, B. Cui, *Microsyst. Nanoeng.* **2019**, *5*, 41.
[39] P. P. Samant, M. R. Prausnitz, *Proc. Natl. Acad. Sci.* **2018**, *115*, 4583.
[40] R. P. Brannigan, A. P. Dove, *Biomater. Sci.* **2017**, *5*, 9.
[41] X. Q. You, Q. Y. He, T. W. Wu, D. Y. Huang, Z. Z. Peng, D. Y. Chen, Z. Chen, J. Liu, *Microchem. J.* **2023**, *190*, 108570.
[42] G. Ye, W. Wang, D. Fan, P. He, *Appl. Surf. Sci.* **2021**, *538*, 148117.
[43] P. Rytlewski, W. Mróz, M. Żenkiewicz, J. Czwartos, B. Budner, *J. Mater. Process. Technol.* **2012**, *212*, 1700.
[44] H. N. Nguyen, C. F. Zhao, O. Millet, A. P. Selvadurai, *Powder Technol.* **2021**, *378*, 487.
[45] R. Liu, A. Li, Y. Lang, H. Cai, X. Tang, D. Li, X. Liu, J. Liu, *J. Drug Deliv. Sci. Technol.* **2023**, *88*, 104922.
[46] K. Park, S. Kim, Y. Jo, J. Park, I. Kim, S. Hwang, Y. Lee, S. Y. Kim, J. Seo, *Bioact. Mater.* **2023**, *25*, 555.
[47] D. Al Sulaiman, J. Y. Chang, N. R. Bennett, H. Topouzi, C. A. Higgins, D. J. Irvine, S. Ladame, *ACS Nano* **2019**, *13*, 9620.
[48] C. W. Lou, C. H. Yao, Y. S. Chen, T. C. Hsieh, J. H. Lin, W. H. Hsing, *Text. Res. J.* **2008**, *78*, 958.
[49] D. Da Silva, M. Kaduri, M. Poley, O. Adir, N. Krinsky, J. Shainsky-Roitman, A. Schroeder, *Chem. Eng. J.* **2018**, *340*, 9.
[50] F. D'Hermies, C. Hartmann, F. Von Ey, C. Holzkämper, G. Renard, Y. Pouliquen, *Fortschritte der Ophthalmologie, Zeitschrift der Deutschen Ophthalmologischen Gesellschaft* **1991**, *88*, 790.
[51] M. Arora, E. K. Chan, S. Gupta, A. D. Diwan, *World J. Orthoped.* **2013**, *4*, 67.
[52] R. Gautam, R. D. Singh, V. P. Sharma, R. Siddhartha, P. Chand, R. Kumar, *J. Biomed. Mater. Res. Part B, Appl. Biomater.* **2012**, *100*, 1444.
[53] D. C. Schohn, H. A. Jahn, M. Eber, G. Hauptmann, *Blood Purif.* **1986**, *4*, 102.
[54] J. G. Turner, E. Lay, U. Jungwirth, V. Varenko, H. S. Gill, P. Estrela, L. HS, *Adv. Mater. Technol.* **2023**, *8*, 2300259.
[55] S. L. Timchenko, E. N. Zadorozhnyi, In2024 6th Int. Youth Conf. on Radio Electronics, Electrical and Power Engineering (REEPE), Moscow, Russian Federation, February **2024**.
[56] N. Bitinis, R. Verdejo, E. M. Maya, E. Espuche, P. Cassagnau, M. A. Lopez-Manchado, *Compos. Sci. Technol.* **2012**, *72*, 305.
[57] Q. Jiang, Y. Du, L. Zhang, W. Ma, F. Yan, L. Zhang, S. Zhao, *Molecules* **2021**, *26*, 863.
[58] E. Chibowski, K. Terpilowski, *Appl. Surf. Sci.* **2009**, *256*, 1573.
[59] S. T. Hsu, H. Tan, Y. L. Yao, 30th Int. Congress on Laser Materials Processing, Laser Microprocessing and Nanomanufacturing, Orlando, Florida, USA, October **2011**.
[60] J. Madden, C. O'Mahony, M. Thompson, A. O'Riordan, P. Galvin *Biosensing in Dermal Interstitial Fluid using Microneedle Based Electrochemical Devices*, Elsevier, Amsterdam **2020**.
[61] S. Peia, S. Babity, A. S. Cordeiro, D. Brambilla, *Adv. Drug Delivery Rev.* **2024**, *210*, 115341.
[62] M. Gilanyi, C. Ikrenyi, J. Fekete, K. Ikrenyi, A. G. Kovach, *Am. J. Physiol.-Renal Physiol.* **1988**, *255*, F513.
[63] J. Zhu, X. Zhou, H. J. Kim, M. Qu, X. Jiang, K. Lee, L. Ren, Q. Wu, C. Wang, X. Zhu, P. Tebon, *Small* **2020**, *16*, 1905910.
[64] M. Razzaghi, A. Seyfoori, E. Pagan, E. Askari, A. Hassani Najafabadi, M. Akbari, *Polymers* **2023**, *15*, 1389.
[65] Y. Yin, X. Li, M. Wang, G. Ling, P. Zhang, *Int. J. Biol. Macromol.* **2024**, *277*, 134408.
[66] Z. Bao, S. Lu, D. Zhang, G. Wang, X. Cui, G. Liu, *Adv. Healthcare Mater.* **2024**, *13*, 2303511.
[67] R. He, H. Liu, T. Fang, Y. Niu, H. Zhang, F. Han, B. Gao, F. Li, F. Xu, *Adv. Sci.* **2021**, *8*, 2103030.
[68] G. Bamorovat Abadi, M. Bahrami, *Sci. Rep.* **2022**, *12*, 14867.
[69] J. Yang, J. Yang, X. Gong, Y. Zheng, S. Yi, Y. Cheng, Y. Li, B. Liu, X. Xie, C. Yi, L. Jiang, *Adv. Healthcare Mater.* **2022**, *11*, 2102547.
[70] H. Kim, J. Lee, U. Heo, D. K. Jayashankar, K. C. Agno, Y. Kim, C. Y. Kim, Y. Oh, S. H. Byun, B. Choi, H. Jeong, *Sci. Adv.* **2024**, *10*, adk5260.
[71] L. Qian, F. Jin, Z. Wei, T. Li, Z. Sun, C. Lai, J. Ma, R. Xiong, X. Ma, F. Wang, F. Sun, *Adv. Funct. Mater.* **2023**, *33*, 2209407.


© 2025 The Author(s). Advanced Materials Interfaces published by Wiley-VCH GmbH

21967350, 2025, 13, Downloaded from https://advanced.onlinelibrary.wiley.com/doi/10.1002/admi.202500001 by Koc University, Wiley Online Library on [10/11/2025]. See the Terms and Conditions (https://onlinelibrary.wiley.com/terms-and-conditions) on Wiley Online Library for rules of use; OA articles are governed by the applicable Creative Commons License